doi:10.1016/j.jmb.2010.06.069 J. Mol. Biol. (2010) 401, 906–920

JMB

Available online at www.sciencedirect.com

ScienceDirect

ELSEVIER

Dimeric Crystal Structure of Rabbit L-Gulonate 3-Dehydrogenase/λ-Crystallin: Insights into the Catalytic Mechanism

Yukuhiko Asada[1], Chizu Kuroishi[2], Yoko Ukita[2], Rie Sumii[3], Satoshi Endo[3], Toshiyuki Matsunaga[3], Akira Hara[3] and Naoki Kunishima[1]*

[1]*Protein Crystallography Research Group, RIKEN SPring-8 Center, Harima Institute, 1-1-1 Kouto, Sayo-cho, Sayo-gun, Hyogo 679-5148, Japan*

[2]*SR System Biology Research Group, RIKEN SPring-8 Center, Harima Institute, 1-1-1 Kouto, Sayo-cho, Sayo-gun, Hyogo 679-5148, Japan*

[3]*Laboratory of Biochemistry, Gifu Pharmaceutical University, Mitahora-higashi, Gifu 502-8585, Japan*

Received 31 March 2010; received in revised form 24 June 2010; accepted 30 June 2010
Available online 8 July 2010

L-Gulonate 3-dehydrogenase (GDH) is a bifunctional dimeric protein that functions not only as an NAD^+-dependent enzyme in the uronate cycle but also as a taxon-specific λ-crystallin in rabbit lens. Here we report the first crystal structure of GDH in both apo form and NADH-bound holo form. The GDH protomer consists of two structural domains: the N-terminal domain with a Rossmann fold and the C-terminal domain with a novel helical fold. In the N-terminal domain of the NADH-bound structure, we identified 11 coenzyme-binding residues and found 2 distinct side-chain conformers of Ser124, which is a putative coenzyme/substrate-binding residue. A structural comparison between apo form and holo form and a mutagenesis study with E97Q mutant suggest an induced-fit mechanism upon coenzyme binding; coenzyme binding induces a conformational change in the coenzyme-binding residues Glu97 and Ser124 to switch their activation state from resting to active, which is required for the subsequent substrate recruitment. Subunit dimerization is mediated by numerous intersubunit interactions, including 22 hydrogen bonds and 104 residue pairs of van der Waals interactions, of which those between two cognate C-terminal domains are predominant. From a structure/sequence comparison within GDH homologues, a much greater degree of interprotomer interactions (both polar and hydrophobic) in the rabbit GDH would contribute to its higher thermostability, which may be relevant to the other function of this enzyme as λ-crystallin, a constitutive structural protein in rabbit lens. The present crystal structures and amino acid mutagenesis studies assigned the role of active-site residues: catalytic base for His145 and substrate binding for Ser124, Cys125, Asn196, and Arg231. Notably, Arg231 participates in substrate binding from the other subunit of the GDH dimer, indicating the functional significance of the dimeric state. Proper orientation of the substrate-binding residues for catalysis is likely to be maintained by an interprotomer hydrogen-bonding network of residues Asn196, Gln199, and Arg231, suggesting a network-based substrate recognition of GDH.

Keywords: 3-hydroxyacyl-CoA dehydrogenase; coenzyme; induced fit; X-ray crystallography; site-directed mutagenesis

Edited by R. Huber

Introduction

L-Gulonate 3-dehydrogenase (GDH; EC 1.1.1.45) is an NAD^+-dependent enzyme in the uronate cycle, an alternative glucose metabolic pathway that plays essential roles in the biosynthesis of glucuronide, glycosaminoglycan, and ascorbic acid. The enzyme oxidizes L-gulonate to 3-dehydro-L-

*Corresponding author. E-mail address: kunisima@spring8.or.jp.

Abbreviations used: GDH, L-gulonate 3-dehydrogenase; λCRY, λ-crystallin; HAD, 3-hydroxyacyl-CoA dehydrogenase; PDB, Protein Data Bank; ASA, accessible surface area; WT, wild type.

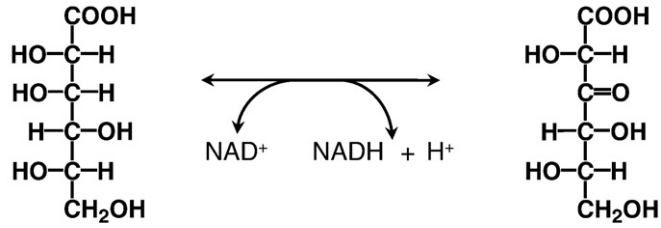

Fig. 1. The reaction catalyzed by GDH.

gulonate (Fig. 1) and is distributed in a variety of tissues of mammals[1–3] and *Drosophila melanogaster*.[4] GDH exhibits additional dehydrogenase activity towards several other organic acids with 3-hydroxyl groups, such as L-3-hydroxybutyrate and L-threonate,[1,4] and is also called L-β-hydroxyacid dehydrogenase. Recently, a cDNA sequence for GDH from rabbit liver[5] was demonstrated to be identical with that of the taxon-specific λ-crystallin (λCRY), which is a constitutive structural protein in rabbit lens.[6] Thus, in rabbits, GDH is a bifunctional protein. In humans, however, GDH is distributed in nonlens tissues, and its expression level is downregulated in hepatocellular carcinoma tissues from patients.[7] Although the GDHs from rabbits and humans share a high sequence identity (84%) and are almost identical in enzymatic properties and molecular sizes as a homodimer of 36-kDa subunits,[5] the rabbit enzyme is remarkably stable against heat/urea denaturation when compared to the human enzyme.

Mammalian GDH shares a marginal sequence identity of around 20% with the NAD^+-dependent 3-hydroxyacyl-CoA dehydrogenase (HAD), an enzyme critical for oxidative fatty-acid metabolism in mammals.[8] To date, crystal structures of HADs from humans and pigs have been reported.[9,10] HAD is also dimeric, and its subunit consists of two distinct domains: N-terminal and C-terminal domains that are responsible for coenzyme binding and subunit dimerization, respectively. Based on the crystal structure of the human HAD/NAD^+/acetoacetyl-CoA ternary complex, Barycki *et al.* proposed a catalytic mechanism of HAD[11] in which His158 was implicated as a general base to abstract a proton from the 3-hydroxyl group of substrate, Glu170 neutralized the positive charge on His158 after the proton abstraction, Ser137 interacted with the substrate and coenzyme to orient them for catalysis, and Asn208 stabilized the reaction product together with Ser137. However, a later study using mutagenesis and crystallography suggested that Glu170 was not directly involved in the catalysis but was required for the proper orientation of the catalytic His158 and for the structural integrity of the human enzyme.[12] The roles of other active-site residues of HAD, including Ser137 and Asn208, should be investigated further.

In spite of the low sequence identity between GDH and HAD, the catalytically important residues (His158, Ser137, Glu170, and Asn208) of human HAD are completely conserved in rabbit and human GDHs (His145, Ser124, Glu157, and Asn196, respectively). A site-directed mutagenesis study of the rabbit GDH has shown that His145, Asn196, and Ser124 are critical for the catalytic function of this enzyme.[5] This supports an earlier suggestion that λCRY/GDH belongs to the same structural family of HADs.[6] However, interestingly, replacement of Glu157 with Gln did not result in apparent kinetic alterations on the rabbit GDH, in contrast to a significant decrease in the activity of the human HAD by a corresponding mutation of Glu170 to Gln.[12] Therefore, further information based on the crystal structure of GDH would provide better understanding and characterization of the functional nature of this nascent group of enzymes. In this study, we present the first crystal structures of rabbit GDH in both apoenzyme form and NADH-bound holoenzyme form at resolutions of 1.70 and 1.85 Å, respectively, to clarify the structural difference between GDH and HAD, as well as to identify the residues of GDH that are crucial for coenzyme specificity, substrate recognition, and catalytic mechanism.

Results and Discussion

Quality of the models

The crystal structure of the rabbit GDH apoenzyme was determined at 1.70 Å resolution, yielding final R_{cryst} and R_{free} factors of 18.3% and 20.6%, respectively. The asymmetric unit contains a monomeric protomer of the enzyme. The final model of the apoenzyme structure covers amino acid residues 7−316 with well-defined electron densities, while six N-terminal residues and three C-terminal residues were not modeled due to structural disorder. A total of 419 water molecules were included in the final refinement. In a stereochemistry analysis using the program PROCHECK,[13] no residue is found in generously allowed or disallowed regions of the Ramachandran plot, with the exception of Phe193, which resides neatly in well-defined electron densities without steric clashes. The crystal structure of the enzyme in complex with NADH was determined at 1.85 Å resolution, yielding final R_{cryst} and R_{free} factors of 16.8% and 20.0%, respectively. The final model of the NADH-bound holoenzyme contains a GDH protomer (residues 7−316), an NADH molecule, and 452 water molecules in the

Table 1. Summary of refinement statistics

	Apoenzyme	NADH bound
Space group	*C*2	*C*2
Resolution range (Å)	30.0–1.70 (1.78–1.70)	30.0–1.85 (1.93–1.85)
Cell dimensions		
a (Å)	71.81	72.02
b (Å)	69.08	69.52
c (Å)	65.64	65.10
β (°)	102.7	102.7
Number of unique reflections	34,455 (4274)	26,578 (3246)
R_{cryst} (%)[a]	18.3 (25.2)	16.8 (20.1)
R_{free} (%)[b]	20.6 (27.6)	20.0 (22.2)
Wilson *B*-factor (Å^2)	22.5	18.9
Average *B*-factor (Å^2)[c]	20.0	16.2
Ramachandran geometry		
Most favored (%)	93.0	91.9
Allowed (%)	6.6	7.4
Generously allowed (%)	0.4	0.4
Disallowed (%)	0.0	0.4
rmsd from ideality		
Bond length (Å)	0.005	0.006
Bond angles (°)	1.2	1.2
Dihedral (°)	20.9	20.2
Improper (°)	0.81	0.83

[a] $R_{cryst} = \sum | F_{obs}(hkl) - F_{calc}(hkl) | / \sum | F_{obs}(hkl) |$.
[b] R_{free} is R_{cryst} calculated for 5% of the data set not included in the refinement.
[c] Protein atoms were used for the calculation.

asymmetric unit. The nine terminal residues are disordered as seen in the apoenzyme structure. With the exception of Asp8 and Phe193, which locate neatly in well-defined electron densities without steric clashes, no other residue is found in generously allowed or disallowed regions of the Ramachandran plot. Statistics from crystallographic analysis are summarized in Table 1. Structural descriptions herein, if not stated differently, denote those observed in the 1. 85-Å crystal structure of the enzyme–NADH complex.

Overall structural architecture

The GDH protomer consists of two distinct domains: the N-terminal α/β dinucleotide-binding domain (residues 7–185) and the C-terminal α-helical domain (residues 195–316) (Fig. 2a). The N-terminal domain contains eight β-strands (β1–β8) and seven α-helices (α1–α7), and displays a typical α/β dinucleotide binding motif, the so-called Rossmann fold.[14] The first six strands of the β-sheet are in a parallel orientation, and the remaining two strands (β7 and β8) run in the opposite direction. In the N-terminal domain, the first six strands are surrounded by exterior α-helices to form a hydrophobic core. Of the loops connecting consecutive secondary structures, the α2–α3 and β6–β7 loops are spatially located in close proximity to each other, in contrast with their distant relationship in primary structure. This loop–loop contact is mediated by the hydrogen-bonding interactions of Lys63 (backbone O and N^{ζ}) with Tyr151 (O^{η} and backbone O, respectively) and 10 hydrophobic contacts between their side-chain carbons within van der Waals distance (Supplementary Fig. 3). Lys63 and Tyr151 are conserved in rabbit, human, and mouse GDHs (Fig. 3). The C-terminal domain of rabbit GDH adopts a novel entirely helical architecture (Fig. 2a) and dominates subunit dimerization. The first six α-helices (α8–α12) form a tightly packed bundle with the cognate α-helices of the other subunit, whereas the terminal long helix α13 somewhat protrudes from the core bundle (Fig. 4; Supplementary Fig. 1). The central helix α8 penetrates the core bundle completely to reach the N-terminal domain of the other subunit, which allows remarkable intersubunit interactions between α9a of one subunit and β8 of the other subunit. In addition, α11 is uniquely bent by approximately 45° at Ser256, when compared to the other straight helices. The two domains are connected by a linker region (β8–α8 loop, residues 186–194), which adopts a hairpin-like conformation (Fig. 2a and b). This conformation is stabilized by eight hydrogen-bonding interactions (Supplementary Table 1). In addition, 31 residue pairs of van der Waals interactions also contribute to the connection of the two domains (Supplementary Table 2). These residues are well conserved in other mammalian GDHs (Fig. 3).

A structural similarity search using the DALI server[15] was performed between the refined model of rabbit GDH protomer and the coordinates available in the Protein Data Bank (PDB). The search did not provide any overall structural homologue. Instead, another DALI analysis using the N-terminal domain of the rabbit GDH as search query identified a number of oxidoreductases: human HAD[9] (PDB accession code 2HDH; *Z*-score = 18.6; rmsd = 1.6 Å), *Aquifex aeolicus* prephenate dehydrogenase[16] (PDB accession code 2G5C; *Z*-score = 16.7; rmsd = 2.4 Å), *Streptococcus pyogenes* Δ^1-pyrroline-5-carboxylate reductase[17] (PDB accession code 2AHR; *Z*-score = 14.3; rmsd = 2.6 Å), *Pseudomonas aeruginosa* class I acetohydroxy acid isomeroreductase[18] (PDB accession code 1NP3; *Z*-score = 14.3; rmsd = 2.6 Å), and *Thermus thermophilus* HB8 3-hydroxy-isobutyrate dehydrogenase[19] (PDB accession code 2CVZ; *Z*-score = 14.0; rmsd = 2.5 Å). These enzymes show a low sequence identity (<21%) with the rabbit GDH and are characterized by an N-terminal Rossmann fold and an enzyme-specific C-terminal domain. Thus, a DALI analysis using the C-terminal domain of the rabbit GDH did not provide any significant similarity with known structures (*Z*-scores <2.6). When the C^{α} trace of the rabbit GDH is compared with that of the human HAD, the N-terminal domain and the domain linker region are well superimposed onto each other, with the exception of the differences in the length of the α3 helix and in the orientation of the α2–α3 loop (Fig. 2c). By contrast, the structures of the C-terminal domains are quite different between these two enzymes, in good agreement with the fact that their sequence identity is low especially in the C-terminal regions (Fig. 3).

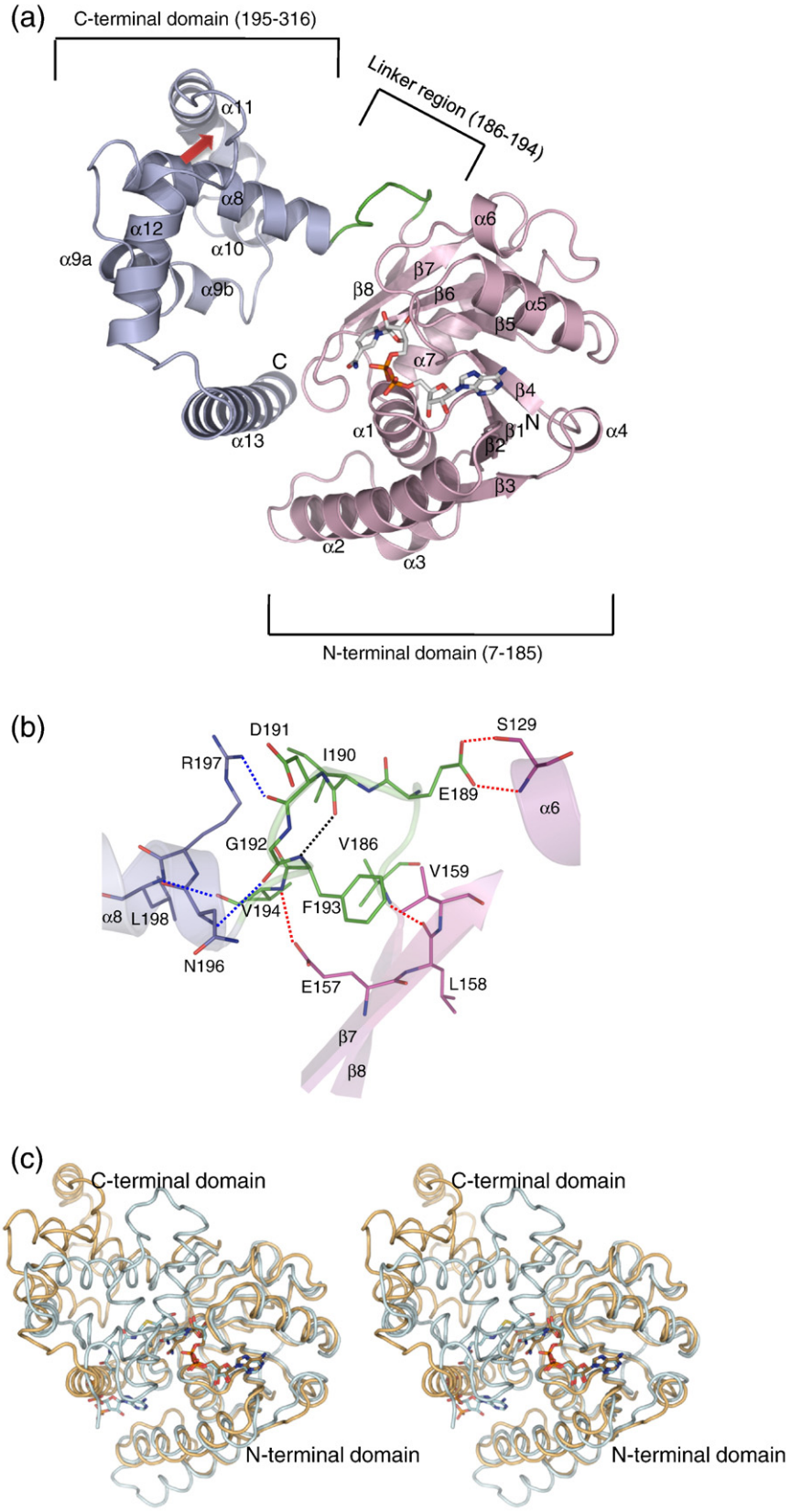

Fig. 2. Structure of rabbit GDH protomer. (a) Ribbon drawing of the NADH-bound GDH structure. The N-terminal domain, the linker region, and the C-terminal domain are shown in pink, green, and light blue, respectively. The NADH molecule bound is shown as a stick model. The bent helix α11 is indicated by a red arrow. (b) Close-up view of the linker region. The residues in linker form hydrogen bond (dotted lines) to those in the N-terminal domain (red), the C-terminal domain (blue), and the linker region (black). (c) Stereo representation of the C^{α} trace of GDH (brown) superimposed onto the structure of human HAD (cyan). The NADH molecule bound in GDH and NAD^{+} and the acetoacetyl-CoA molecule bound in HAD are depicted as stick models.

Dimerization interface

Interprotomer interactions in the crystal lattice clearly suggest that the rabbit GDH assembles into an apparent dimer (Fig. 4; Supplementary Fig. 1). This observed crystal-state dimer is consistent with our previous biochemical study that used a gel-filtration method, which revealed that the enzyme functions as a homodimer in solution state.[5] The dimeric structure can be generated by applying a

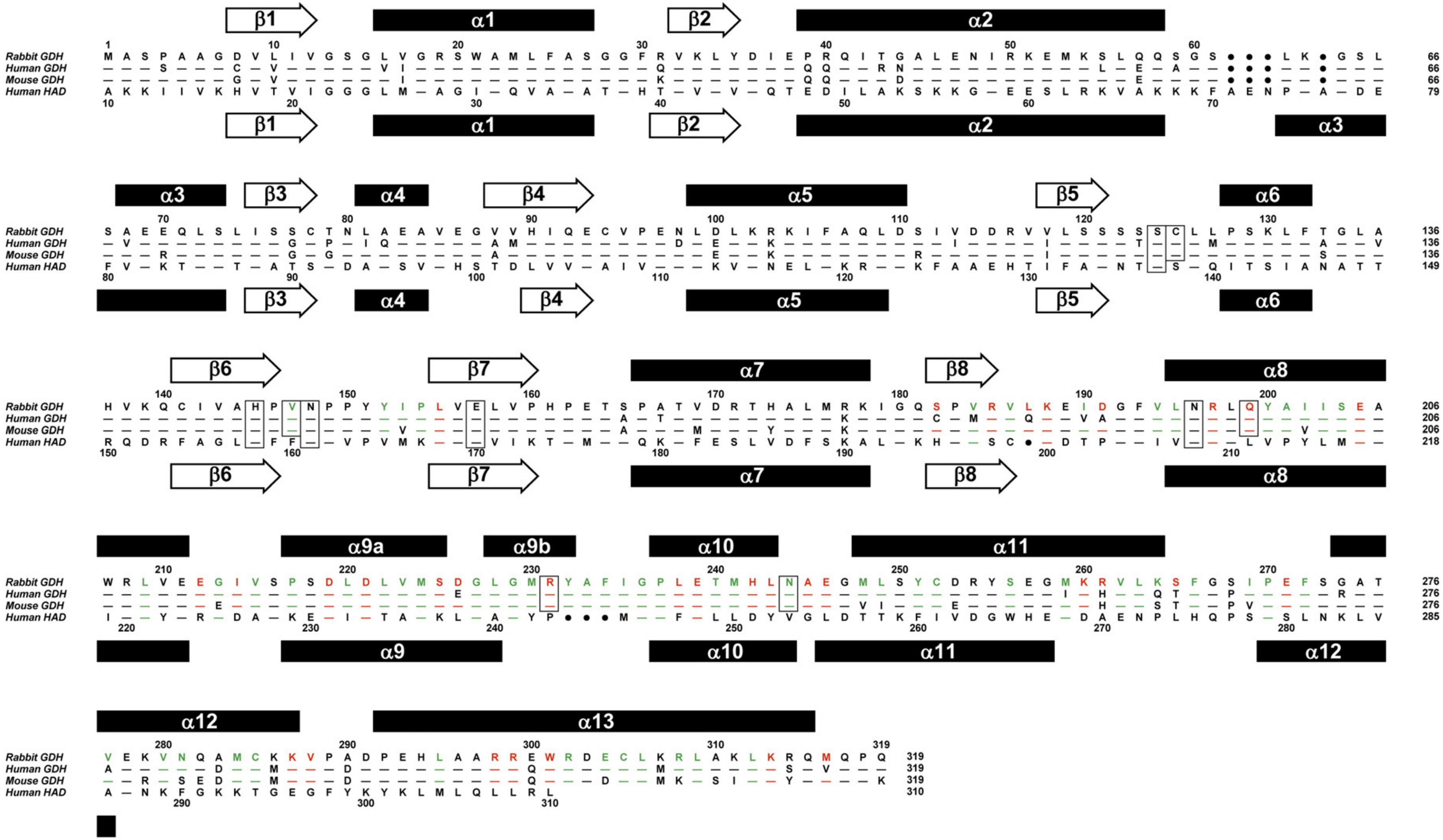

Fig. 3. Structure-based sequence alignments of rabbit GDH with homologues. The amino acid sequence of the rabbit GDH (accession no. AB359905) was aligned with those of the human GDH (accession no. AK024041), mouse GDH (accession no. AB359906), and human HAD (accession no. 2515250A). Residues identical with those of the rabbit GDH are denoted by hyphens. Alignment gaps are indicated by closed circles. The N-terminal mitochondrial targeting signal (nine residues) of HAD is excluded. Secondary structure elements of the rabbit GDH and the human HAD are depicted above and below their sequences, respectively. Functionally important residues in the rabbit GDH are boxed. The dimer interface residues are distinguished by colors: red, residues involving both hydrogen bonds and van der Waals interactions (33 residues); green, residues involving only van der Waals interactions (61 residues).

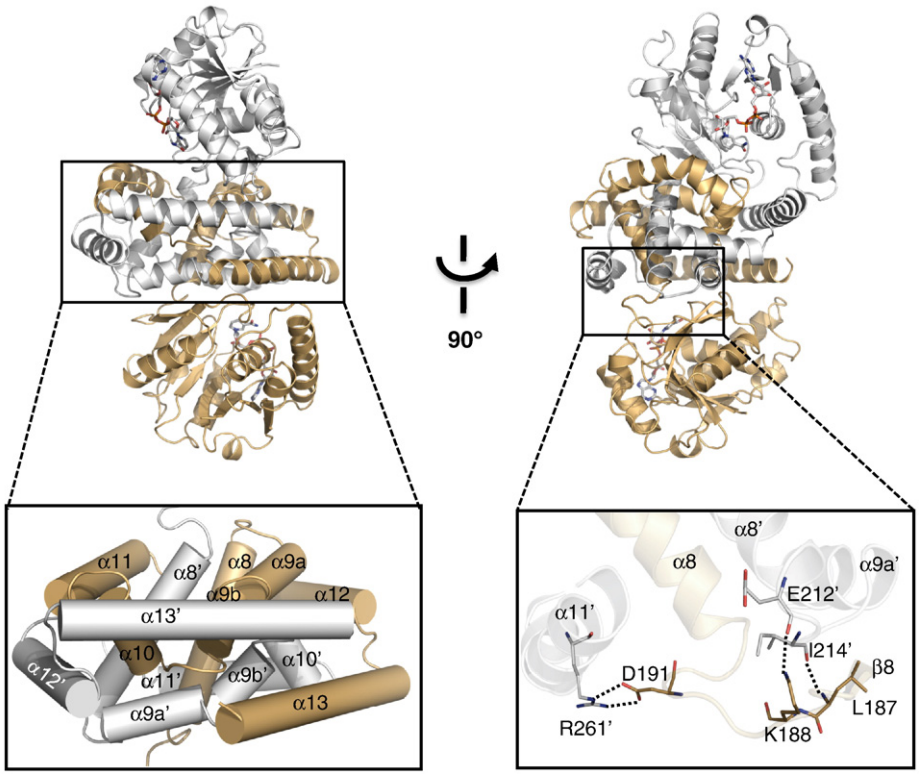

Fig. 4. Diagrams of the GDH homodimer showing important intersubunit interactions. The right model is rotated by 90° with respect to the left. One subunit is shown in brown, and the other subunit is shown in gray. Bound NADH molecules are depicted as stick models. The enlargement (box) on the left is a cylinder drawing of the C-terminal dimerization domain. The enlargement on the right shows a ribbon drawing of the linker region and nearby helices on the other subunit. Hydrogen-bonding interactions are indicated by dotted lines.

crystallographic 2-fold symmetry operation to the protomer in the asymmetric unit. Thus, we define a prime as representing an affiliation with the other subunit of the crystal-state dimer with a perfect 2-fold axis. A molecular surface analysis using the program Connolly[20] shows that 5186 Å^2 of accessible surface area (ASA) per protomer is buried by the dimer interface. The buried area at the dimer interface corresponds to 29.6% or 55.9% of ASA for the total protomer or the C-terminal domain, respectively, suggesting a tight dimer association. Subunit dimerization is mediated by numerous intersubunit interactions, including 22 hydrogen bonds and 104 residue pairs of van der Waals interactions (Supplementary Tables 3 and 4).

Subunit dimerization of GDH is mediated by residues mainly on the C-terminal domain through interprotomer homodomain (C-domain to C-domain) interactions. C-domain helices are arranged so as to make anti-parallel helical pairs between α8 and α8′, α9 and α9′, and α13 and α13′ (Fig. 4, left). Interface interactions at the central helical pair (α8–α8′) are maintained by a hydrogen bond between Arg197 and Glu205′ and by four residue pairs of van der Waals interactions between Arg197 and Glu205′/Leu209′, Ala201 and Ala201′, Ile202 and Ile202′. Residues on α8 also interact with those in the other structural elements of the counterpart subunit through 2 hydrogen bonds at Arg197 and Gln199 and 18 residue pairs of van der Waals interactions. It should be noted that the side chain of Gln199 forms an interprotomer hydrogen-bonding network with putative substrate-binding residues Asn196 and Arg231′, whose possible role will be discussed in a later section. Although the terminal helix α13 (residues 292–315) is located away from the main body of the C-domain core (α8–α12), it contributes to subunit association through many interactions with the C-domain residues on the other subunit. These interactions include 7 hydrogen bonds and 23 residue pairs of van der Waals interactions. Other helices and loops in the C-terminal domain also make interprotomer homodomain interactions, including 5 hydrogen bonds and 34 residue pairs of van der Waals interactions.

Part of the N-terminal domain (β7 and β8) and the linker region (β8–α8 loop) are additionally involved in subunit dimerization through interprotomer heterodomain interactions, including 7 hydrogen bonds and 25 residue pairs of van der Waals interactions. Noteworthy, the charged hydrogen bonds between Asp191 and Arg261′ may stabilize the bent conformation of α11′ (Fig. 4, right).

Thermostabilization of rabbit GDH

The number of intraprotomer hydrogen bonds of the rabbit GDH and the human HAD is 358 and 342, respectively. The number of intraprotomer

electrostatic interactions of the rabbit GDH and the human HAD is 8 and 11, respectively. These data suggest that the contribution of intraprotomer hydrogen bonding or intraprotomer electrostatic interactions to the thermal stability of the rabbit GDH is similar to their contribution to the human HAD. On the other hand, the numerous interprotomer interactions at the dimer interface of the rabbit GDH, including 22 hydrogen bonds, are in contrast to much fewer interactions at the human HAD interface in which only 4 hydrogen bonds are present.[9] In addition, a unique feature for the rabbit GDH is the involvement of the linker region (β8–α8 loop) in dimerization through interprotomer heterodomain interactions including 4 hydrogen bonds. In this region of the human HAD, only Lys200 and Asp226′ make a hydrogen bond,[9] which corresponds to that formed by Lys188 and Glu212′ in the rabbit GDH. Moreover, the ratio of the dimer interface area to the C-terminal domain surface area in the rabbit GDH (55.9%) is much higher than that in the human HAD (32.3%). These structural comparisons suggest that the dimer association of the rabbit GDH is much stronger than that of the human HAD.

Unfortunately, there is no report of an experimental comparison of the folding stabilities of the rabbit GDH and the human HAD. In order to estimate quantitatively the thermal stability of these proteins, we calculated semiempirically the Gibbs energy differences (ΔG) upon denaturation from hydrophobic interactions (Table 2). The ΔG values for the rabbit GDH were higher than those for the human HAD by 65, 992, and 864 kJ/mol in the monomeric state, dimeric state, and dimer interface, respectively. These data show that hydrophobic interactions are stronger in the rabbit GDH than in the human HAD, especially when the dimer interfaces are compared.

On the other hand, within mammalian GDHs, the human enzyme is reported to be much less stable against denaturation by heat or urea when compared to the rabbit enzyme.[5] As shown in alignments of their amino acid sequences (Fig. 3), 7 residues required for interprotomer hydrogen-bonding interactions (Ser182, Leu187, Asp191, Asp226, Arg261, Ser265, and Met316) and 12 residues required for interprotomer hydrophobic interactions (Ser182, Val184, Leu187, Ile190, Asp191, Asp226, Met259, Arg261, Lys264, Ser265, Val277, and Met316) in the rabbit GDH are not conserved in the human enzyme. Particularly, the replacement of Asp191 and Arg261 with Ala and His, respectively, in the human GDH may impair the dimer interface between the β8–α8 loop and the α11 helix, since the strong interactions between Asp191 and Arg261 would contribute substantially to dimer stability (Fig. 4, right). Collectively, a much greater degree of interprotomer interactions (both polar and hydrophobic) in the rabbit GDH is likely to enhance its thermostability as compared with the homologous proteins. The higher stability of the rabbit GDH may be favorable for its other function as the taxon-specific λCRY, which is a constitutive structural protein probably requiring such extra thermostabilization.

Table 2. Contribution of hydrophobicity to thermal stability

	Monomeric state		Dimeric state		Dimer interface	
Protein	ΔG	$\Delta\Delta G$	ΔG	$\Delta\Delta G$	ΔG	$\Delta\Delta G$
Rabbit GDH (3ADO)	2995	0	7255	0	1266	0
Human HAD (1F14)	2930	−65	6263	−992	402	−864

ΔG and $\Delta\Delta G$ values are expressed in kilojoules per mole. PDB accession codes used for the calculation are expressed in parentheses. See Materials and Methods in detail.

Coenzyme binding mode

In the structure of GDH complexed with NADH, the coenzyme is bound to the Rossmann fold of the N-terminal domain with well-defined electron densities (Fig. 5a). The NADH-binding residues 13–18 represent a consensus sequence Gly-X-Gly-X-X-Gly, which is one of the amino acid fingerprints for NAD(P) binding.[14,21] A C^{α} superposition between the apoenzyme model and the NADH-bound model provided an rmsd of 0.2 Å. Significant deviations upon NADH binding are observed in the N-terminal regions of α1 and α2 and in the β6–α6 loop. Especially, the side-chain orientations of Leu16, Val17, Arg40, Gln41, Glu97, Ser124, and Cys125 are different between the two forms (Fig. 5b). Among these residues, the side chains of Gln41, Glu97, and Ser124 are directly involved in coenzyme binding. While the $N^{\varepsilon 2}$ of Gln41 is hydrogen bonded to the carboxylate of Asp36 in the apoenzyme, it makes a hydrogen bond with the 3′-OH of the adenine ribose of NADH and interacts with the pyrophosphate moiety of coenzyme via a water molecule (Fig. 5b and c). The carboxylate oxygen atoms $O^{\varepsilon 1}$ and $O^{\varepsilon 2}$ of Glu97 are hydrogen bonded to the O^{γ} of Ser123 and the backbone N of Ser124, respectively, in the apoenzyme. In the NADH-bound structure, the conformation of the Glu97 side chain is significantly changed so that its carboxylate forms additional interactions with the nicotinamide ribose and Cys125 (Figs. 5c and 6). The protein–coenzyme hydrogen bonds are summarized in Fig. 5c. These residues, except for Leu16 and Val17, are conserved in other mammalian GDHs (Fig. 3). A hydrogen bond is found between the side chain of Asn148 and the carboxyamide oxygen of the nicotinamide moiety, which is also recognized by the protein main chains (Leu16 and Ser20) via a water molecule. The hydroxyl groups of the nicotinamide ribose interact with the side chains of Lys102, Glu97, and Ser124. The pyrophosphate moiety interacts with residues 14–18. The hydroxyl groups of the adenine ribose are recognized by the carboxylate of Asp36, in addition to the above-mentioned recognition by Gln41. There is no polar interaction between the adenine moiety and the protein residues.

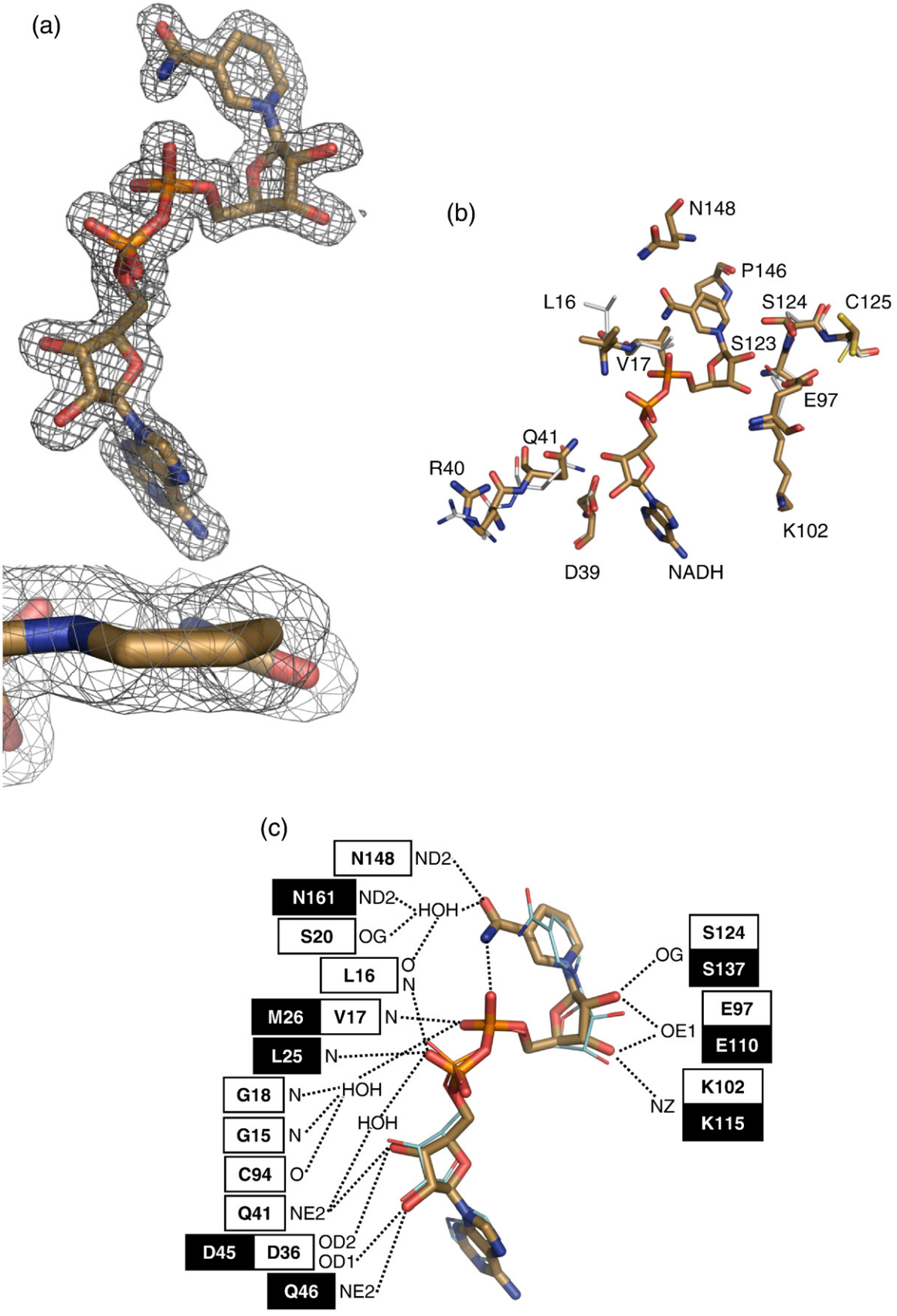

Fig. 5 *(legend on next page)*

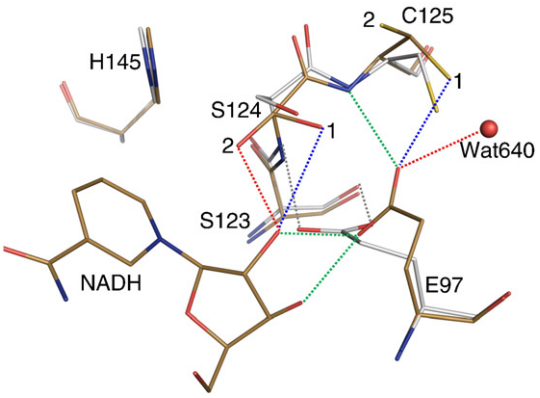

Fig. 6. Alternative conformations of Ser124 and Cys125 in the rabbit GDH. The active-site residues are superimposed: the apoenzyme form (gray) and the NADH-bound form (brown). The side-chain conformation of Glu97 is different between the two forms; its torsion angles $\chi 1$ and $\chi 2$ in the NADH-bound form are $-175°$ and 75°, respectively, whereas the respective values are $-67°$ and $-66°$ in the apoenzyme form. In the NADH-bound form, the side chains of Ser124 and Cys125 show two alternate conformations: conformer-1 and conformer-2. Hydrogen-bonding interactions specifically derived from conformer-1 and conformer-2 are represented as dotted lines shown in blue and red, respectively. The remaining constitutive hydrogen bonds among the nicotinamide ribose, Glu97, and Cys125 are shown in green dotted lines. In the apoenzyme model, two hydrogen bonds among Glu97, Ser123, and Ser124 are indicated by gray dotted lines.

Bound NADH molecule adopts an extended form in which the adenine moiety is in *anti* conformation and the nicotinamide moiety is in *syn* conformation. Both ribose rings have C2′-*endo* puckering. The bottom panel in Fig. 5a shows an enlarged view of the pyridine ring of nicotinamide. Fortunately, a high resolution of the crystal structure clearly revealed a boat conformation of the pyridine ring, indicative of the reduced state of the coenzyme. The carboxyamide nitrogen of nicotinamide forms a self-hydrogen bond (2.95 Å) with one of the pyrophosphate oxygens (Fig. 5c). Notably, the B-face of the nicotinamide ring is exposed to the putative substrate-binding pocket, whereas the A-face packs against nonpolar residues Val17 and Pro146 (Fig. 5b). In addition, the *syn* conformation of the nicotinamide ring is observed in the crystal structures of human HAD[9] and other oxidoreductases[22] that transfer the B-face 4-*pro*-S hydride ion. Thus, from a structural point of view, GDH would be a B-side-specific dehydrogenase, although no biochemical data on its reaction stereochemistry are available to date.

In our previous report, the role of Asp36 in coenzyme specificity was partly understood with its replacement with arginine in the D36R mutant, which showed dual coenzyme specificity for both NAD^+ and $NADP^+$.[5] To establish the roles of the newly identified coenzyme-binding residues in the current crystallographic study, we replaced Gln41 and Glu97 with Asn and Gln, respectively. In addition, the double-mutant enzyme D36R/Q41N was prepared to examine cooperation between Asp36 and Gln41 in coenzyme specificity. The kinetic alterations by these mutations are summarized in Table 3. The single mutation E97N virtually abolished enzyme activity, indicating a critical role for Glu97 in catalysis. On the other hand, the single mutation Q41N had few effects on the steady-state kinetics for both L-gulonate and $NAD(P)^+$. However, the double mutation D36R/Q41N resulted in an almost complete switch of coenzyme specificity; the NAD^+-linked reaction showed a large decrease in V_{max}/K_m value, whereas a significant increase was observed in the $NADP^+$-linked reaction. The ratio of V_{max}/K_m for the $NADP^+$-linked reaction to the NAD^+-linked reaction was 48, which was much higher than the values for mutations D36R and Q41N (9.5 and 0.005, respectively). This indicates a synergistic effect between Asp36 and Gln41 for the determination of cofactor specificity, through their cooperative interactions with the hydroxyl groups of the adenine ribose, although the contribution may be predominant in Asp36.

Induced fit of Ser124 and Cys125 upon coenzyme binding

Interestingly, in the NADH-bound crystal, the side chains of Ser124 and neighboring Cys125 show considerable extra electron densities (Supplementary Fig. 4), indicating the existence of two alternative side-chain conformations: conformer-1 and conformer-2. Such conformers were observed neither in other residues of the holoenzyme structure nor in all residues of the apoenzyme structure that was solved at a slightly higher resolution. The conformer-1 O^γ of Ser124, which is similar to that in the apoenzyme, is hydrogen bonded to the 2′-OH of the nicotinamide ribose (3.17 Å), but is positioned away from the catalytic base His145 (Fig. 6). By contrast, in conformer-2 of Ser124, the C^α–C^β bond rotates by about 120° when compared to conformer-1, allowing the O^γ atom to locate more closely to both the 2′-OH of nicotinamide ribose (2.67 Å) and

Fig. 5. Coenzyme binding modes. (a) The final $(2F_o-F_c)$ electron density at 1.85 Å resolution contoured at 2σ for the NADH molecule in the rabbit GDH/NADH complex. The coenzyme model is shown as a stick model. The bottom panel shows an enlarged view of the pyridine ring of NADH. (b) Comparison of residues around the coenzyme-binding pocket in the apoenzyme (gray) and the GDH/NADH complex (brown). The coenzyme and residues are depicted as stick models. (c) Schematic representation of the NADH binding mode in rabbit GDH and human HAD. A cyan wire NADH model of the HAD/NADH complex (PDB accession code 1F17) is superimposed on a brown stick NADH model of the GDH/NADH complex. Potential hydrogen bonds are indicated with broken lines. Shaded boxes represent corresponding residues in HAD.

Table 3. Alteration of kinetic parameters for coenzymes and L-gulonate by mutations

Parameter	WT[a]	D36R[a]		Q41N		D36R/Q41N		E97Q	
		Value	Ratio[b]	Value	Ratio[b]	Value	Ratio[b]	Value	Ratio[b]
NAD^+-linked activity									
K_m NAD^+ (mM)	0.010	1.3	130	0.028±0.001	3	2.6±0.4	260	0.054±0.06	5
K_m l-gulonate (mM)	0.18	14	78	1.3±0.1	7	3.3±0.3	19	1.6±0.1	9
V_{max} (U/mg)	3.1	1.3	0.4	5.9±0.2	2	0.65±0.02	0.2	0.007±0.001	0.002
V_{max}/K_m NAD^+	314	1.0	0.003	209	0.7	0.25	0.0006	0.13	0.0004
$NADP^+$-linked activity									
K_m $NADP^+$ (mM)	0.67	0.20	0.3	0.86±0.13	1	0.12±0.01	0.1	ND[c]	—
K_m L-gulonate (mM)	2.4	18	8	14±1.2	6	2.6±0.2	1	ND[c]	—
V_{max} (U/mg)	0.36	1.9	5	0.83±0.02	2	1.5±0.1	3	ND[c]	—
V_{max}/K_m $NADP^+$	0.54	9.5	17	0.97	2	12	22	ND[c]	—
$NADP^+/NAD^+$ ratio of V_{max}/K_m	0.001	9.5	9500	0.005	5	48	48,000	—	—

[a] Taken from Ishikura *et al.*[5]
[b] Ratio of mutant to WT.
[c] Activity was not detectable.

the catalytic base. In the neighboring Cys125, the conformer-1 S^γ locates within a hydrogen-bonding distance (2.98 Å) of the $O^{\varepsilon 2}$ of Glu97. However, in conformer-2 of Cys125, the C^α–C^β bond rotates similarly to Ser124, resulting in relocation of the S^γ atom to occupy a cavity space created by the 1-to-2 conformational change in Ser124. Related cavity formation by the 1-to-2 conformational change in Cys125 is compensated for by the recruitment of a water molecule, Wat640, that forms a new hydrogen bond with the $O^{\varepsilon 2}$ of Glu97 (2.93 Å). Notably, *B*-factor values of these residues do not increase upon NADH binding, indicating an unchanged degree of flexibility (Table 4). Therefore, coenzyme binding most likely provides additional conformer-2 to Ser124 and Cys125, rather than destabilizing the structure of these residues. In our previous report, a mutagenesis study suggested a critical role for Ser124 in the catalytic function of GDH.[5] Furthermore, the conformer-2 O^γ of Ser124 is located within hydrogen-bonding distance of the 3-OH of the modeled substrate L-gulonate, as described in a later section. Therefore, the side chain of Ser124 would move to its conformer-2 state from its conformer-1 state in the enzyme reaction, which helps subsequent substrate binding.

Since the N-terminal domains of the rabbit GDH and the human HAD are structurally similar, their coenzyme binding modes are compared by superposition (Fig. 5c). Although the conformations of NADH molecules in the two enzymes are generally similar, slight differences are observed in the orientations of the nicotinamide moiety. This is probably due to a difference in recognition residues for the carboxyamide moiety of nicotinamide: three residues Leu16, Ser20, and Asn148 in GDH, and only Asn161 in HAD.[9,11] In addition, the interaction of Gln41 with the hydroxyl groups of the adenine ribose in the GDH structure differs from that of the corresponding residue (Gln46) of HAD. The coenzyme-binding residues of GDH outnumber those of HAD. This may be relevant to the higher cofactor affinity of GDH compared to that of HAD; the dissociation constants at pH 7.0 for NAD^+ and NADH in GDH are 16 and 0.4 μM, respectively,[5] whereas the corresponding values in HAD are 86 and 0.7 μM.[9] Furthermore, the coenzyme-induced conformational change in Ser124 found in this study was not observed in the studies of human HAD.[9,11,12] In our comparison of the human HAD crystal structures, including the apoenzyme form (PDB accession code 1F14), NADH-bound form

Table 4. Occupancy and *B*-factor of atoms relevant to NADH binding

		NADH bound		Apoenzyme	
	Atom	Occupancy	*B*-factor (Å^2)	Occupancy	*B*-factor (Å^2)
Ser124	N	1.0	12.25	1.0	13.14
	C^α	1.0	13.61	1.0	13.46
	C	1.0	14.35	1.0	15.37
	O	1.0	15.62	1.0	16.36
	C^β	1.0	13.91	1.0	16.63
	O^γ conformer-1	0.5	15.45	1.0	18.63
	O^γ conformer-2	0.5	13.25	—	—
Cys125	N	1.0	15.63	1.0	16.37
	C^α	1.0	18.20	1.0	19.91
	C	1.0	15.91	1.0	19.10
	O	1.0	17.78	1.0	22.78
	C^β	1.0	20.15	1.0	21.67
	S^γ conformer-1	0.5	26.80	1.0	32.84
	S^γ conformer-2	0.5	24.42	—	—
Glu97	N	1.0	11.15	1.0	18.61
	C^α	1.0	11.23	1.0	20.29
	C	1.0	12.19	1.0	20.44
	O	1.0	12.07	1.0	22.01
	C^β	1.0	10.17	1.0	21.50
	C^γ	1.0	11.50	1.0	25.21
	C^δ	1.0	11.93	1.0	24.39
	$O^{\varepsilon 1}$	1.0	10.90	1.0	25.30
	$O^{\varepsilon 2}$	1.0	13.17	1.0	26.96
NADH[a]		1.0	13.71	—	—

[a] Forty-four atoms were used for the calculation.

(PDB accession code 1F17), and NAD^+-bound form (PDB accession code 3HAD), the side chain of Ser137, corresponding to the Ser124 of GDH, shows only one conformation, which is not similar to the two conformers seen in the GDH/NADH complex. By contrast, the orientation of the Ser137 side chain in the human HAD/NAD^+/acetoacetyl-CoA ternary complex (PDB accession code 1F0Y) is almost identical with that of the conformer-2 Ser124 of GDH, further supporting that conformer-2 is the catalytically active state of Ser124. Thus, the proposed conformational change in Ser124 induced by coenzyme binding may be a unique and important step in GDH catalysis.

The role of Glu97 in GDH catalysis is intriguing because it also shows a substantial conformational change upon coenzyme binding (Fig. 6). Notably, in the present mutagenesis study, the E97Q mutation only moderately affects the coenzyme K_m, but results in an increase in substrate K_m and a marked drop in V_{max}. This clearly suggests the role of Glu97 as a trigger for the conformational changes in Ser124 and Cys125 in the coenzyme induced-fit mechanism proposed. The reaction catalyzed by GDH follows the compulsory ordered mechanism, in which the coenzyme binds to the enzyme first and leaves last.[5] The current findings provide structural evidence on the mechanistic steps of the ordered binding of the coenzyme and substrate, although determination of the ternary complex will be needed to completely understand the coenzyme induced-fit mechanism.

Active site and substrate recognition

A putative GDH active site was identified as an interdomain pocket that is adjacent to the nucleotide-binding site (Fig. 7a). Structural information on the enzyme–NADH complex facilitated this identification process. The nicotinamide moiety of NADH and the catalytically important residues Ser124, His145, and Asn196 are found in this pocket. Importantly, the putative active site is located at the dimerization interface; a large portion of the binding pocket is maintained by one subunit, including the regions of the β6−α6 loop, β6, β7, and α8, whereas α9b′ and the α10′−α11′ loop complete the pocket in the other subunit. Analysis of this pocket revealed a highly polar active site accommodating a small hydrophilic substrate molecule. Briefly, Ser124, Cys125, His145, Val147, and Asn148 are found at the base of the pocket, whereas Asn196, Gln199, Arg231′, and Asn244′ line the walls of the active site. These nine residues are conserved in rabbit, human, and mouse GDHs.

To gain further insight into the interactions between the substrate and GDH, we modeled an L-gulonate molecule into the putative active site (Fig. 7b) using structural information from the active-site residues and the C-4 atom of nicotinamide moiety as guide. In particular, the positions of residues His145 and Arg231 were useful in orienting the 3-hydroxyl group and the carboxyl group, respectively, of L-gulonate molecule, since the equivalent histidine residue in the human HAD (His157) has been assigned as the catalytic base involved in hydride transfer[11] and since Arg231 is suggested in this study as a key residue that binds the carboxylate moiety of gulonate. The modeled substrate molecule resides in the positively charged active-site pocket of the rabbit GDH dimer. The C-3 atom of L-gulonate is considered as the reactive center, since the hydride at this position should be transferred to the C-4 atom of NAD^+ during the enzymatic reaction to produce the product 3-dehydro-L-gulonate (Fig. 1). Thus, L-gulonate was modeled into the putative active site so that its C-3 is 3.4 Å away from the C-4 atom of coenzyme. The L-gulonate C-3 hydroxyl points toward His145 and Ser124 and is located within potential hydrogen-bonding distances of these two residues.

Reaction mechanism of GDH involving a network-based substrate recognition

In our previous mutagenesis study on the rabbit GDH, the H145Q mutation produced an inactive enzyme, and the S124A mutation resulted in significant decreases in substrate affinity and V_{max} value.[5] The crucial roles of His145 and Ser124 as catalytic base and substrate/product-binding residue, respectively, are further confirmed by the present observation of these residues in the crystal structure and by the modeling study of the substrate complex. While the imidazole ring of His145 does not interact with the side chain of Ser124, it is positioned to form a hydrogen bond with a carboxylate oxygen of Glu157 (Fig. 7a). However, in our previous report, the mutagenesis of E157Q did not result in a significant alteration of kinetic constants for the coenzyme and the substrate, except that it caused a subtle impairment in the heat stability of the enzyme.[5] To clarify the interaction between His145 and Glu157, we replaced Glu157 of the rabbit GDH with Asp or Asn, in which one-carbon-shorter side chains would split potential hydrogen bonds between these two residues. As a result, both E157D and E157N mutants were found to be inactive enzymatically, although their intrinsic fluorescence was decreased by the addition of NAD(H), indicative of their ability to bind the coenzyme. This suggests that Glu157 participates in the proper orientation of the imidazole ring of the catalytic base His145 by forming a hydrogen bond. Probably, no interaction with the His145 side chain is present in the E157D and E157N mutants, whereas $O^{\varepsilon 1}$ of the replaced Gln in the E157Q mutant is still capable of forming an effective hydrogen bond with the imidazole ring of His145 to orient the catalytic base. Thus, a properly oriented His145 seems to work as the catalytic base without any assistance from acidic or hydroxyl amino acids in the GDH reaction. This is similar to the recently modified catalytic mechanism of human HAD,[12] but differs from that of the catalytic His-Asp dyad for glucose 6-phosphate dehydrogenases[23] and malate/lactate dehydrogenases,[24] and from that of the catalytic

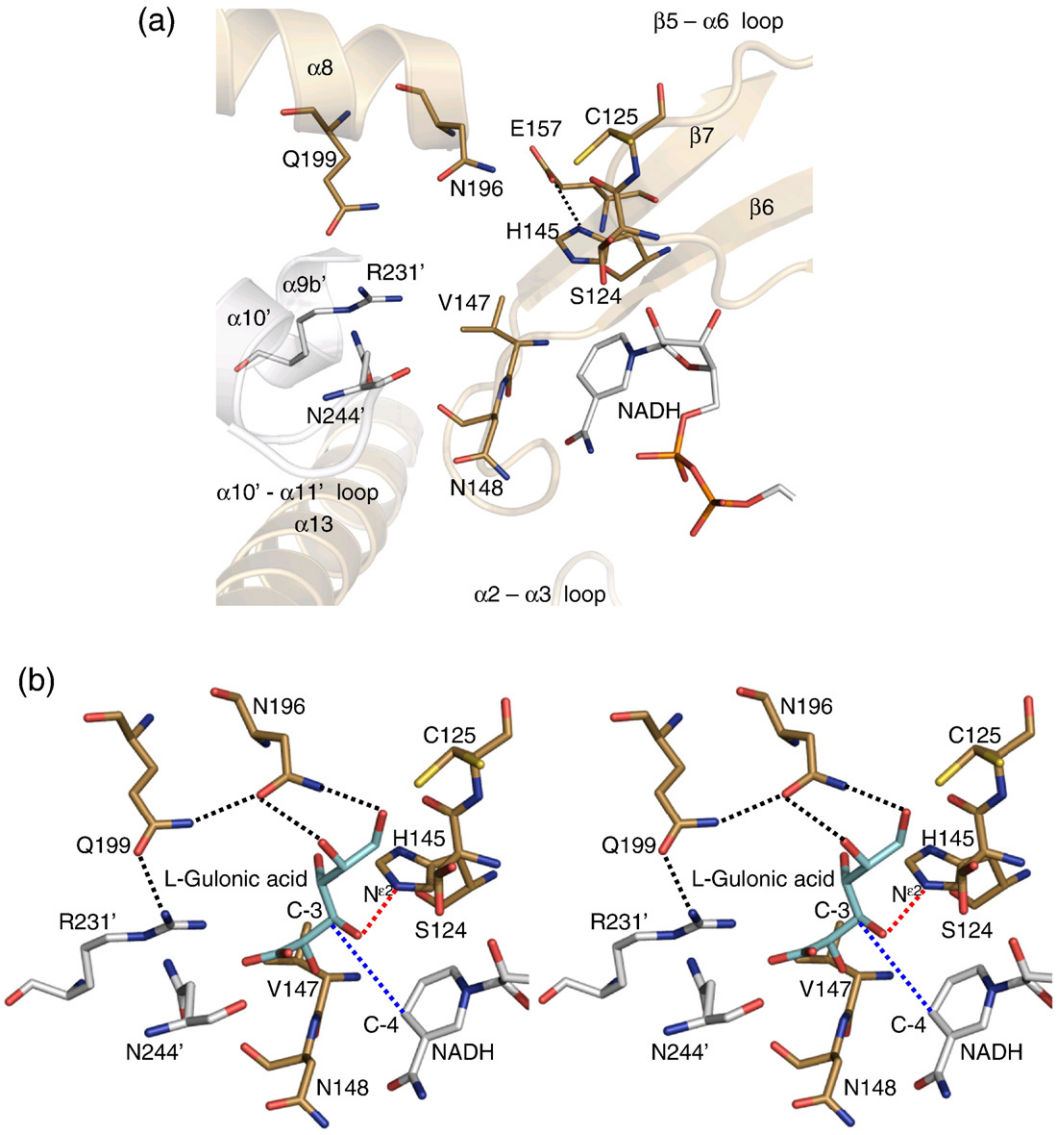

Fig. 7. Putative GDH active site at the domain/subunit interface. Secondary structural elements (ribbons) and residues from one subunit are shown in brown, and those from the other subunit and NADH are shown in gray. (a) Diagram of the active-site residues. The residues and the NADH molecule are depicted as stick models. A dotted line indicates the hydrogen bond between the imidazole ring of His145 and the carboxylate of Glu157. (b) Close-up view of the modeled L-gulonate molecule (light blue), the surrounding protein residues, and the NADH molecule. Hydrogen-bonding network among Asn196, Gln199, and Arg231′, as well as possible hydrogen bonds between the substrate and the protein residues, is shown as black dotted lines. The blue dotted line represents a putative hydride transfer pathway. The red dotted line represents a putative proton transfer pathway.

His-Ser-Asp triad for enzymes in the new NAD(P)-dependent oxidoreductases family.[25]

It was reported that a mutation at Asn196 of the rabbit GDH into Asp or Gln also produces almost inactive enzymes.[5] In the current crystal structure, Asn196 is far (>5 Å) away from His145, and its side chain $N^{\delta 2}$ is hydrogen bonded to the C-5 and C-6 hydroxyls of the modeled L-gulonate (Fig. 7b). Notably, we identified a hydrogen-bonding network among the side chains of Asn196 and Gln199 from one subunit and the side chain of Arg231 from the other subunit. Since the $N^{\eta 2}$ of Arg231′ is within electrostatic interaction distance of the C-1 carboxylate of the modeled L-gulonate, it is likely that the interprotomer hydrogen-bonding network involving Asn196, Gln199, and Arg231′ conducts the passage of substrate into the active site by assisting with the proper orientation of the side chain of Arg231′. To confirm this hypothesis, we prepared an R231M mutant of GDH and found that it was completely inactive; no enzyme activity was observed from an excess amount (0.2 mg) of homogeneous enzyme preparation. These results, together with the previous mutagenesis study on Asn196, demonstrate the importance of network-based substrate recognition in the regulation of GDH reaction. Since the hydrogen-bonding network involves residues from both subunits, the functional

importance of the dimeric state of GDH is emphasized further.

The GDH/λCRY family

The 10 functionally important residues are perfectly conserved in the rabbit, human, and mouse GDHs, whereas only five residues (Ser124, His145, Asn148, Glu157, and Asn196) are conserved in the human HAD (Fig. 3). These five invariant residues may play common important roles in the reactions of both GDH and HAD. However, while GDH is similar to HAD with respect to their N-terminal domain structures with catalytic amino acids, they quite differ from each other in their C-terminal domain structures, interprotomer interactions, and mechanisms of substrate recognition. For instance, the presence of the large C-terminal helix α13 near the substrate-binding pocket of GDH may explain why this enzyme does not accept large substrate molecules,[1,4,5] unlike HAD, which has a broad substrate specificity for CoA derivatives with 4–16 acyl-chain carbons.[26] Furthermore, although Asn196 is conserved in the human HAD at position 208, the hydrogen-bonding network including this residue for substrate recognition was not observed in the crystal structure of HAD.[11] In addition, the induced-fit mechanism upon coenzyme binding is observed only in GDH. Therefore, our findings cast doubt on the previous assumption that GDH/λCRY and HAD belong to the same enzyme family.[6] Amino acid sequences of the human, rabbit, and mouse GDHs show high full-length identities (>76%) with λCRY homologues from orangutan, dog, pig, cow, and rat (accession nos. Q5RDZ2, XP_543175, NP_999046, AF480862, and AY040223, respectively). Most of the coenzyme-binding residues and active-site residues of rabbit GDH identified in the current study are conserved in these homologues, suggesting their identity in the same family. In conclusion, we propose a new GDH/λCRY family that is distinct from the conventional HAD superfamily. The knowledge presented here will be the molecular basis for understanding the proteins in this new family.

Materials and Methods

Chemicals

Chemicals were purchased from Sigma-Aldrich Chemical Company, Fluka, and Merck. Crystallization kits were purchased from Hampton Research. L-Gulonate was synthesized as described previously.[4]

Assay of enzyme activity

The dehydrogenase activity of rabbit GDH was assayed by measuring the rate of change in coenzyme fluorescence at 455 nm from excitation at 340 nm.[5] The standard reaction mixture consisted of 50 mM 4-morpholinepropanesulfonic acid–NaOH (pH 7.0), 1 mM NAD^+, 10 mM L-gulonate, and enzyme in a total volume of 2.0 ml. One unit of activity was defined as the amount of enzyme that catalyzes the formation of 1 μ mol/min NAD(P)H at 25 °C. The kinetic constants for the coenzymes were determined using a saturating concentration (more than 3-fold of the K_m values) of L-gulonate from experiments performed in triplicate.

Site-directed mutagenesis, expression, purification, and crystallization

Mutagenesis was performed using a QuickChange site-directed mutagenesis kit (Stratagene) and an expression pRset vector harboring the cDNA for rabbit GDH,[5] in accordance with the protocol described by the manufacturer. The mutagenic primers were designed to produce the mutant enzymes of GDH (D36R, Q41N, E97D, E196N, and R231M) by replacing the respective codons in the cDNA with those for the replaced amino acids. The cDNA for D36R/Q41N was similarly prepared by replacing the codon for Gln41 in the D36R mutant cDNA with AAC, using the primers for preparing the Q41N mutant. The complete coding regions of the cDNAs were sequenced with a CEQ2000XL DNA sequencer (Beckman Coulter) to confirm the presence of the desired mutations and to ensure that no other mutation had occurred. The wild-type (WT) and mutated cDNAs were expressed in *Escherichia coli* BL21(DE3) cells, and the recombinant enzymes were purified from 20,000*g* supernatants of cell homogenates (each from 1 L of culture) by assaying L-gulonate dehydrogenase activity or by detecting the 36-kDa protein band by SDS-PAGE, as described previously.[5,27] SDS-PAGE of the purified WT and mutants showed a single protein band corresponding a molecular mass of 36 kDa (Supplementary Fig. 2). The protein concentration was determined by the method of Bradford using bovine serum albumin as protein standard.[28] Crystals of the purified recombinant rabbit GDH and its NADH complex were obtained by the oil microbatch method, as described previously.[29]

Structure determination, refinement, and evaluation

For data collection, crystals were directly mounted on cryoloops from crystallization drops and frozen in cold nitrogen gas stream at 100 K. The diffraction data for the apoenzyme were collected using a Rigaku R-AXIS V image plate detector and synchrotron radiation at beamline BL26B1[30] of SPring-8 (Japan). The diffraction data for the GDH/NADH complex were collected in-house using a Rigaku R-AXIS VII image plate detector and a MicroMax 007 generator operating with a copper target. All measured diffraction spots were indexed, integrated, and scaled using the HKL2000 program package,[31] as described previously.[29]

The rabbit GDH structure in apo form was solved by a molecular replacement technique using the program MOLREP.[32] Chain A of HAD from *Archaeoglobus fulgidus* (PDB accession code 1ZEJ) was used as search model. To minimize the model bias caused by the search model, we applied the initial phase to a phase improvement process using the prime-and-switch protocol implemented in the program RESOLVE.[33] The resultant electron density map was of high quality and clearly interpretable. The atomic model of GDH was built using the graphic program QUANTA (Accelrys, Inc., San Diego, CA, USA) and refined using the program CNS, version 1.1.[34] Several cycles of model building and refinement yielded the final

model. The crystal structure of the rabbit GDH/NADH complex was solved by a difference Fourier technique based on the apoenzyme structure. A model for the NADH molecule bound to the enzyme was built into the difference electron density map, and refinement of the NADH-bound structure was carried out as described for the apoenzyme. The final refinement statistics for the two enzyme forms are given in Table 1. The same set of R_{free} reflections was used for the refinement of both structures. The stereochemical quality of the final structures was checked using the program PROCHECK.[13]

Analysis of the secondary structure was performed with the program DSSP.[35] Fold similarity searches were performed with the DALI server.[14] Superimpositions of protein models were performed using the program LSQKAB.[36] The ASA of protein molecule was calculated using the program Connolly.[20] The denaturation Gibbs energy (ΔG) of a protein due to hydrophobic effect was estimated by the following equation from ASA values of the protein model:[37,38]

$$\Delta G = 0.178\Delta\mathrm{ASA}_{\mathrm{nonpolar}} - 0.013\Delta\mathrm{ASA}_{\mathrm{polar}}$$

where $\Delta\mathrm{ASA}_{\mathrm{nonpolar}}$ and $\Delta\mathrm{ASA}_{\mathrm{polar}}$ represent the differences in ASA values of a protein upon denaturation in nonpolar (C/S) and polar (N/O) atoms, respectively. The ASA value of the native state was calculated from a native crystal structure, and that of the denatured state was calculated from an extended structure that was generated from the native structure using the program Insight II (Accelrys, Inc.). Hydrogen bond was defined as a proper donor–acceptor interaction within a distance range of 2.2 Å$< d \leq$ 3.4 Å. Electrostatic interaction was defined as an interaction between a pair of oppositely charged atoms (Asp/Glu/C-terminus and Arg/Lys/His/N-terminus), with a distance of not more than 5.0 Å. Van der Waals interaction was defined as an interatomic interaction with a distance range of 2.65 Å$< d \leq$ 4.0 Å. All visualization and image production were prepared using the program PyMOL†.

PDB accession numbers

The atomic coordinates and structure factor amplitudes of the rabbit GDH in the apoenzyme form and the NADH-bound form were deposited in the RCSB PDB with accession codes 3ADO and 3ADP, respectively.

Acknowledgements

This work (HTPF50004) was supported by the "National Project on Protein Structural and Functional Analyses" funded by the Ministry of Education, Culture, Sports, Science, and Technology of Japan.

Supplementary Data

Supplementary data associated with this article can be found, in the online version, at doi:10.1016/j.jmb.2010.06.069

† http://pymol.sourceforge.net

References

1. Smiley, J. D. & Ashwell, G. (1961). Purification and properties of β-L-hydroxy acid dehydrogenase: II. Isolation of β-keto-L-gluconic acid, an intermediate in L-xylulose biosynthesis. *J. Biol. Chem.* **236**, 357–364.
2. Koundakjian, P. P. & Snoswell, A. M. (1972). 3-Hydroxy acid dehydrogenases in sheep tissues. *Biochem. J.* **127**, 449–452.
3. Goode, D., Lewis, M. E. & Crabbe, M. J. C. (1996). Accumulation of xylitol in the mammalian lens is related to glucuronate metabolism. *FEBS Lett.* **395**, 174–178.
4. Borack, L. I. & Sofer, W. (1971). *Drosophila* β-L-hydroxy acid dehydrogenase. Purification and properties. *J. Biol. Chem.* **246**, 5345–5350.
5. Ishikura, S., Usami, N., Araki, M. & Hara, A. (2005). Structural and functional characterization of rabbit and human L-gulonate 3-dehydrogenase. *J. Biochem.* **137**, 303–314.
6. Mulders, J. W., Hendriks, W., Blankesteijn, W. M., Bloemendal, H. & de-Jong, W. W. (1988). λ-Crystallin, a major rabbit lens protein, is related to hydroxyacyl coenzyme A dehydrogenases. *J. Biol. Chem.* **263**, 15462–15466.
7. Chen, J., Yu, L., Li, D., Gao, Q., Wang, J., Huang, X. *et al.* (2003). Human CRYL1, a novel enzyme-crystallin overexpressed in liver and kidney and downregulated in 58% of liver cancer tissues from 60 Chinese patients, and four new homologs from other mammalians. *Gene*, **302**, 103–113.
8. Schulz, H. (1991). Beta oxidation of fatty acids. *Biochim. Biophys. Acta*, **1081**, 109–120.
9. Barycki, J. J., O'Brien, L. K., Bratt, J. M., Zhang, R., Sanishvili, R., Strauss, A. W. & Banaszak, L. J. (1999). Biochemical characterization and crystal structure determination of human heart short chain L-3-hydroxyacyl-CoA dehydrogenase provide insights into catalytic mechanism. *Biochemistry*, **38**, 5786–5798.
10. Barycki, J. J., O'Brien, L. K., Birktoft, J. J., Strauss, A. W. & Banaszak, L. J. (1999). Pig heart short chain L-3-hydroxyacyl-CoA dehydrogenase revisited: sequence analysis and crystal structure determination. *Protein Sci.* **8**, 2010–2018.
11. Barycki, J. J., O'Brien, L. K., Strauss, A. W. & Banaszak, L. J. (2000). Crystallographic and spectroscopic evidence for distinct conformations of L-3-hydroxyacyl CoA dehydrogenase. *J. Biol. Chem.* **275**, 27186–27196.
12. Barycki, J. J., O'Brien, L. K., Strauss, A. W. & Banaszak, L. J. (2001). Glutamate 170 of human L-3-hydroxyacyl-CoA dehydrogenase is required for proper orientation of the catalytic histidine and structural integrity of the enzyme. *J. Biol. Chem.* **276**, 36718–36726.
13. Laskowski, R. A., MacArthur, M. W., Moss, D. S. & Thornton, J. M. (1993). PROCHECK: a program to check the stereochemical quality of protein structures. *J. Appl. Crystallogr.* **26**, 283–291.
14. Rossmann, M. G., Moras, D. & Olsen, K. W. (1974). Chemical and biological evolution of nucleotide-binding protein. *Nature*, **250**, 194–199.
15. Holm, L. & Sander, C. (1993). Protein structure comparison by alignment of distance matrices. *J. Mol. Biol.* **233**, 123–138.
16. Sun, W., Singh, S., Zhang, R., Turnbull, J. L. & Christendat, D. (2006). Crystal structure of prephenate dehydrogenase from *Aquifex aeolicus*: insights into the catalytic mechanism. *J. Biol. Chem.* **281**, 12919–12928.

17. Nocek, B., Chang, C., Li, H., Lezondra, L., Holzle, D., Collart, F. & Joachimiak, A. (2005). Crystal structures of Δ^1-pyrroline-5-carboxylate reductase from human pathogens *Neisseria meningitides* and *Streptococcus pyogenes*. *J. Mol. Biol.* **354**, 91–106.
18. Ahn, H. J., Eom, S. J., Yoon, H. J., Lee, B. I., Cho, H. & Suh, S. W. (2003). Crystal structure of class I acetohydroxy acid isomeroreductase from *Pseudomonas aeruginosa*. *J. Mol. Biol.* **328**, 505–515.
19. Lokanath, N. K., Ohshima, N., Takio, K., Shiromizu, I., Kuroishi, C., Okazaki, N. *et al.* (2005). Crystal structure of novel NADP-dependent 3-hydroxyisobutyrate dehydrogenase from *Thermus thermophilus* HB8. *J. Mol. Biol.* **352**, 905–917.
20. Connolly, M. L. (1993). The molecular surface package. *J. Mol. Graphics*, **11**, 139–141.
21. Bellamaciana, C. R. (1996). The nicotinamide nucleotide binding motif: a comparison of nucleotide binding proteins. *FASEB J.* **10**, 1257–1269.
22. Tanaka, N., Nonaka, T., Nakamura, K. T. & Hara, A. (2001). SDR: structure, mechanism of action, and substrate recognition. *Curr. Org. Chem.* **5**, 89–111.
23. Cosgrove, M. S., Naylor, C., Paludan, S., Adams, M. J. & Levey, H. R. (1998). On the mechanism of the reaction catalyzed by glucose 6-phosphate dehydrogenase. *Biochemistry*, **37**, 2759–2767.
24. Goward, C. R. & Nicholls, D. J. (1994). Malate dehydrogenase: a model for structure, evolution, and catalysis. *Protein Sci.* **3**, 1883–1888.
25. Goto, M., Muramatsu, H., Mihara, H., Kurihara, T., Esaki, N., Omi, R. *et al.* (2005). Crystal structures of Δ^1-piperideine-2-carboxylate/Δ^1-pyrroline-2-carboxylate reductase belonging to a new family of NAD(P)H-dependent oxidoreductases. *J. Biol. Chem.* **280**, 40875–40884.
26. Kobayashi, A., Jiang, L. L. & Hashimoto, T. (1996). Two mitochondrial 3-hydroxyacyl-CoA dehydrogenases in bovine liver. *J. Biochem.* **119**, 775–782.
27. Nakanishi, M., Deyashiki, Y., Ohshima, K. & Hara, A. (1995). Cloning, expression and tissue distribution of mouse tetrameric carbonyl reductase. Identity with an adipocyte 27-kDa protein. *Eur. J. Biochem.* **228**, 381–387.
28. Bradford, M. M. (1976). A rapid and sensitive method for the quantitation of microgram quantities of protein utilizing the principle of protein–dye binding. *Anal. Biochem.* **72**, 248–254.
29. Asada, Y., Kuroishi, C., Ukita, Y., Sumii, R., Endo, S., Matsunaga, T. *et al.* (2008). Crystallization and preliminary X-ray crystallographic analysis of rabbit L-gulonate 3-dehydrogenase. *Acta Crystallogr. Sect. F*, **64**, 228–230.
30. Ueno, G., Kanda, H., Hirose, R., Ida, K., Kumasaka, T. & Yamamoto, M. (2006). RIKEN structural genomics beamlines at the SPring-8; high throughput protein crystallography with automated beamline operation. *J. Struct. Funct. Genomics*, **7**, 15–22.
31. Otwinowski, Z. & Minor, W. (1997). Processing of X-ray diffraction data collected in oscillation mode. *Methods Enzymol.* **276**, 307–326.
32. Vagin, A. & Teplyakov, A. (1997). MOLREP: an automated program for molecular replacement. *J. Appl. Crystallogr.* **30**, 1022–1025.
33. Terwilliger, T. C. (2003). SOLVE and RESOLVE automated structure solution and density modification. *Methods Enzymol.* **374**, 22–37.
34. Brünger, A. T., Adams, P. D., Clore, G. M., DeLano, W. L., Gros, P., Grosse-Kunstleve, R. W. *et al.* (1998). Crystallography and NMR system (CNS): a new software suite for macromolecular structure determination. *Acta Crystallogr. Sect. D*, **54**, 905–921.
35. Kabsch, W. & Sander, W. (1983). Dictionary of protein secondary structure: pattern recognition of hydrogen-bonded and geometrical features. *Biopolymers*, **22**, 2577–2637.
36. Kabsch, W. (1976). A solution for the best rotation to relate two sets of vectors. *Acta Crystallogr. Sect. A*, **32**, 922–923.
37. Funahashi, J., Takano, K., Yamagata, Y. & Yutani, K. (1999). Contribution of amino acid substitutions at two different interior positions to the conformational stability of human lysozyme. *Protein Eng.* **12**, 841–850.
38. Tanaka, H., Chinami, M., Mizushima, T., Ogasahara, K., Ota, M., Tsukihara, T. *et al.* (2001). X-ray crystalline structures of pyrrolidone carboxyl peptidase from a hyperthermophile, *Pyrococcus furiosus*, and its Cys-free mutant. *J. Biochem.* **130**, 107–118.